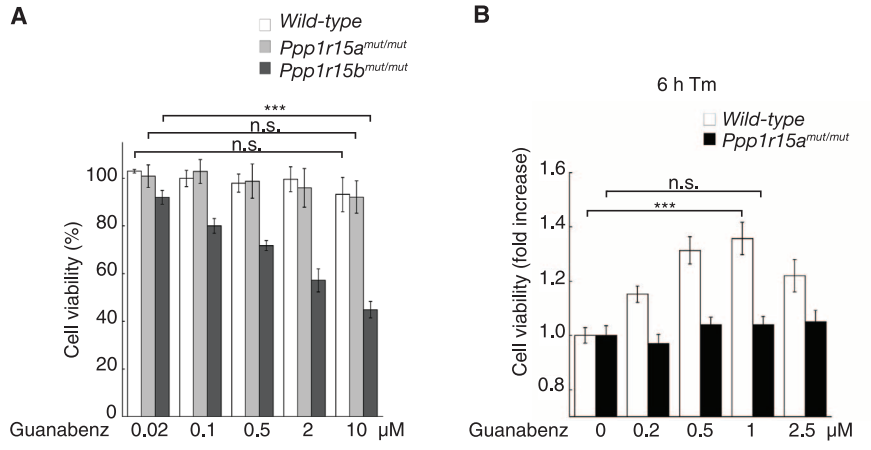

Fig. 4. The ER stress–cytoprotective activity of guanabenz is mediated by inhibition of PPP1R15A. (**A**) Viability of wild-type MEFs or mutant cells (*mut/mut*) lacking PPP1R15A or PPP1R15B activity after exposure to the indicated concentrations of guanabenz for 48 hours. Data are means ± SD ($n = 4$). ***$P \leq 0.0001$; n.s., not significant. (**B**) Viability of wild-type or *Ppp1r15a* mutant (*mut/mut*) MEFs exposed to tunicamycin (1 μg/ml; Tm) for 6 hours with the indicated concentrations of guanabenz, assessed by the ability to reduce WST-8 into formazan. The reducing activity of cells of either genotype exposed to tunicamycin without guanabenz was normalized to 1.

lation of misfolded proteins in the ER. Guanabenz inhibits PPP1R15A and tunes translation in stressed cells to levels manageable by the available chaperones, while sparing PPP1R15B, thereby avoiding intolerable levels of eIF2α phosphorylation (*15*) and deleteriously low levels of protein synthesis (fig. S5). This approach to correcting proteostasis defects by inhibition of PPP1R15A could benefit many conditions characterized by the accumulation of misfolded proteins.

References and Notes

1. D. Ron, P. Walter, *Nat. Rev. Mol. Cell Biol.* **8**, 519 (2007).
2. D. T. Rutkowski, R. J. Kaufman, *Trends Cell Biol.* **14**, 20 (2004).
3. K. Mori, *J. Biochem.* **146**, 743 (2009).
4. W. E. Balch, R. I. Morimoto, A. Dillin, J. W. Kelly, *Science* **319**, 916 (2008).
5. I. Novoa, H. Zeng, H. P. Harding, D. Ron, *J. Cell Biol.* **153**, 1011 (2001).
6. I. Kim, W. Xu, J. C. Reed, *Nat. Rev. Drug Discov.* **7**, 1013 (2008).
7. B. Holmes, R. N. Brogden, R. C. Heel, T. M. Speight, G. S. Avery, *Drugs* **26**, 212 (1983).
8. D. Tribouillard-Tanvier *et al.*, *PLoS One* **3**, e1981 (2008).
9. J. Wang *et al.*, *J. Clin. Invest.* **103**, 27 (1999).
10. M. Liu, I. Hodish, C. J. Rhodes, P. Arvan, *Proc. Natl. Acad. Sci. U.S.A.* **104**, 15841 (2007).
11. I. Novoa *et al.*, *EMBO J.* **22**, 1180 (2003).
12. S. J. Marciniak *et al.*, *Genes Dev.* **18**, 3066 (2004).
13. C. Jousse *et al.*, *J. Cell Biol.* **163**, 767 (2003).
14. A. McCluskey, A. T. Sim, J. A. Sakoff, *J. Med. Chem.* **45**, 1151 (2002).
15. H. P. Harding *et al.*, *Proc. Natl. Acad. Sci. U.S.A.* **106**, 1832 (2009).
16. We thank A. Merritt and C. Wallace for biotinylated guanabenz, J. Hastie for purified recombinant PP1c, anonymous reviewers for suggestions, and M. Goedert for advice on the manuscript. Supported by the UK Medical Research Council. D.R. is a Wellcome Trust Principal Research Fellow. A.B. is a co-inventor on patent WO/2008/041133.

Supporting Online Material

www.sciencemag.org/cgi/content/full/science.1201396/DC1
Materials and Methods
Figs. S1 to S5
References

8 December 2010; accepted 11 February 2011
Published online 3 March 2011;
10.1126/science.1201396

Directional Switching of the Kinesin Cin8 Through Motor Coupling

Johanna Roostalu,[1] Christian Hentrich,[2]* Peter Bieling,[2]† Ivo A. Telley,[2] Elmar Schiebel,[1]‡ Thomas Surrey[2]‡§

Kinesin motor proteins are thought to move exclusively in either one or the other direction along microtubules. Proteins of the kinesin-5 family are tetrameric microtubule cross-linking motors important for cell division and differentiation in various organisms. Kinesin-5 motors are considered to be plus-end–directed. However, here we found that purified kinesin-5 Cin8 from budding yeast could behave as a bidirectional kinesin. On individual microtubules, single Cin8 motors were minus-end–directed motors, whereas they switched to plus-end–directed motility when working in a team of motors sliding antiparallel microtubules apart. This kinesin can thus change directionality of movement depending on whether it acts alone or in an ensemble.

Kinesins are microtubule-binding motor proteins required for essential intracellular movements (*1*). They are known to be unidirectional, and their directionality depends on how the motor domain is linked to the remainder of the molecule (*2*, *3*). Kinesins with an N-terminal motor domain move toward the plus end of microtubules, whereas C-terminal kinesins are minus-end–directed (*4*). The directionality of intracellular transport processes is thought to be regulated by selective recruitment or activation of different sets of motors with characteristic, built-in directionalities (*1*).

Kinesin-5 is an N-terminal homotetrameric kinesin that cross-links microtubules (*5*, *6*). Purified vertebrate kinesin-5 is plus-end–directed and slides antiparallel microtubules apart in vitro (*7*), which is consistent with its role in the mitotic spindle. Budding yeast possesses two largely redundant kinesin-5 proteins, with Cin8 being the more prominent one (*8*, *9*). Apart from its role in spindle assembly (*8*, *9*), Cin8 is required for kinetochore positioning in metaphase (*10*, *11*) and for spindle elongation during anaphase, when it localizes to overlapping antiparallel microtubules in the spindle midzone (*11*–*13*).

We purified recombinant full-length Cin8 fused to monomeric green fluorescent protein (mGFP) (Fig. 1A) (*14*). Cin8-mGFP was a tetramer (table S1 and fig. S1), as expected (*5*). Using total internal reflection fluorescence (TIRF) microscopy, we examined the behavior of single Cin8 tetramers on individual immobilized microtubules in vitro (Fig. 1, B and C, fig. S2, and movie S1). Cin8 motility displayed a combination of directional and diffusive modes as revealed by means of kymographs (time-space plots) (Fig. 1D) and confirmed through mean square displacement (MSD) analysis (Fig. 1E) (*14*). The one-dimensional diffusion coefficient was 0.03 $\mu m^2/s$, and the directional drift speed was 101.7 nm/s. This composite motility is similar to the single-motor behavior of vertebrate kinesin-5 (*15*). However, in contrast to other kinesin-5 family members and all other natural N-terminal kinesins, single

[1]Zentrum für Molekulare Biologie der Universität Heidelberg, DKFZ-ZMBH Allianz, Im Neuenheimer Feld 282, Heidelberg 69120, Germany. [2]Cell Biology and Biophysics Unit, European Molecular Biology Laboratory, Meyerhofstrasse 1, 69117 Heidelberg, Germany.

*Present address: Howard Hughes Medical Institute, Department of Molecular Biology and Center for Computational and Integrative Biology, Massachusetts General Hospital, Boston, MA 02114, USA.

†Present address: Department of Cellular and Molecular Pharmacology, University of California, San Francisco, San Francisco, CA 94158, USA.

‡To whom correspondence should be addressed. E-mail: e.schiebel@zmbh.uni-heidelberg.de (E.S.); thomas.surrey@cancer.org.uk (T.S.)

§Present address: Cancer Research UK London Research Institute, Lincoln's Inn Fields Laboratories, 44 Lincoln's Inn Fields, London WC2A 3LY, UK.

Cin8 motors clearly moved on average toward microtubule minus ends (Fig. 1, C and D, and fig. S2). Mean displacement (MD) analysis (Fig. 1F) revealed that individual Cin8 motors were minus-end–directed, with an average speed of 58 nm/s (Fig. 1F). This difference in speed obtained from either MSD or MD analysis was due to the broad displacement distribution (fig. S2D) (*14*). Minus-end–directed motility of single Cin8 tetramers was an inherent feature of adenosine 5′-triphosphate (ATP)–dependent motor activity because in the presence of ADP, Cin8 displayed only diffusive motion without any directional bias (fig. S3) with reduced dwell times (Fig. 1G). Thus, Cin8 represents an N-terminal kinesin that moves toward the microtubule minus end.

In vivo Cin8 extends the yeast anaphase spindle through plus-end–directed antiparallel microtubule sliding (*13*, *16*). To test whether Cin8 might switch directionality of movement when cross-linking two microtubules, we generated antiparallel microtubule pairs of differently fluorescently labeled and polarity-marked microtubules (*17*). One of the microtubules in a pair

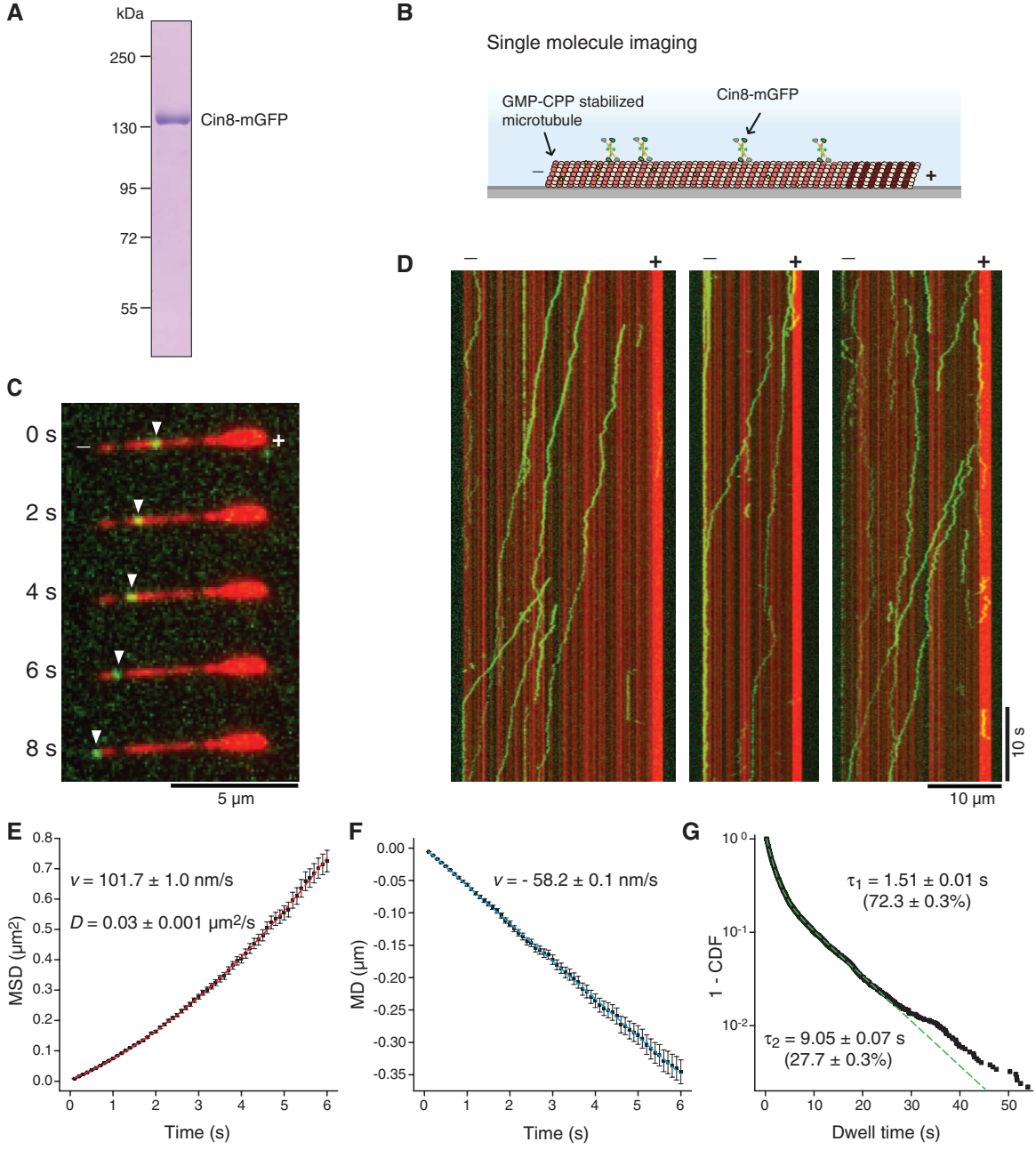

Fig. 1. Single Cin8 motors on individual microtubules are minus-end–directed. (**A**) Coomassie-stained SDS–polyacrylamide gel electrophoresis (SDS-PAGE) of purified recombinant Cin8-mGFP. (**B**) Scheme of the single-molecule assay. (**C**) Example frames of a TIRF microscopy time-lapse movie showing (green; white arrowheads) Cin8-mGFP movement on (red) a surface-immobilized Alexa568-labeled polarity-marked microtubule with a bright plus end and a dim minus end. (**D**) Representative kymographs of (green) Cin8-mGFP movement on (red) Alexa568-labeled polarity-marked microtubules. (**E** to **G**) Quantification of 5000 individual Cin8-mGFP binding events on polarity-marked microtubules. Mean velocities (*v*) and the diffusion constant (*D*) were derived by fitting the following functions to (E) MSD and (F) MD data: (dashed red line) $MSD = v^2t^2 + 2Dt + offset$ and (dashed blue line) $MD = vt$. (G) Mean dwell times (τ) and relative amplitudes (in brackets) were obtained from fitting a bi-exponential function (dashed green line) to the measured dwell time distribution [shown as 1 − cumulative distribution function (CDF)]. Cin8-mGFP was used at 20 to 30 pM. Stated errors and error bars represent SEM.

was surface-immobilized, whereas the other was cross-linked to it by Cin8-mGFP (Fig. 2, A and B) (*14*). Cin8-mGFP accumulated in antiparallel microtubule overlap regions (Fig. 2B and movie S2). Antiparallel microtubules always moved with their plus end lagging, which is indicative of plus-end–directed Cin8 motility (Fig. 2C), as observed for *Xenopus* kinesin-5 (*7*, *17*). The measured sliding velocities (16-17 nm/s) (Fig. 2D) agreed well with the speed of the first, Cin8-dependent phase of anaphase spindle elongation in vivo (around 15 nm/s) (*12*). Furthermore, we observed Cin8-mGFP accumulation at minus ends of single microtubules outside the overlap regions (Fig. 2, B and C), confirming that under identical conditions, but in a different context, Cin8 moved toward the minus end. Thus, although single Cin8 motors are minus-end–directed on individual microtubules (Figs. 1 and 2, B and C) teams of Cin8 motors cross-linking antiparallel two microtubules move toward the plus end. Cin8 thus behaves as a bidirectional motor whose directionality depends on the microtubule-motor configuration.

The switch in Cin8 directionality could be caused, for example, by communication between the two ends of the tetramer when cross-linking two microtubules or, alternatively, by a collective phenomenon: Multiple motors simultaneously binding to an antiparallel microtubule pair could influence each other. We performed microtubule gliding experiments in which multiple surface-immobilized motors collectively transport microtubules (Fig. 3A). Immobilized purified Cin8 motors were found to be plus-end–directed (Fig. 3B and movie S3), which is in agreement with previous gliding assays with surface-adsorbed Cin8 from crude yeast extract (*18*). The speed derived from MSD and MD analysis was between 4 and 5 nm/s (Fig. 3B). Thus, Cin8 does not need to cross-link two microtubules to be plus-end–directed. Next, we reduced the surface density of Cin8 by lowering the protein concentration from 250 to 10 nM and keeping buffer conditions constant. This resulted in fast, minus-end–directed motility, with intermittent pause phases (speeds of 50 nm/s and 31.9 nm/s from MSD and MD analysis, respectively) (Fig. 3D and movie S3). At intermediate motor concentrations (50 nM), microtubule transport was bidirectional, showing phases of both plus- and minus-end–directed motility (Fig. 3C and movie S3) with characteristic switching times in the range of a minute (fig. S4). The speed of transport depended on the nucleotide concentration (fig. S5). As expected for such heterogeneous motility, the transport speeds deduced from MSD (13 nm/s) versus MD (3.8 nm/s) analysis (Fig. 3C) varied considerably. The switch in the directionality depended also on microtubule length (Fig. 3E). This demonstrates that not the density itself but rather the number of motors interacting with a microtubule critically determines the direction of transport. Therefore, large Cin8 ensembles that are mechanically coupled via surface attachment switch to plus-end–directed motility.

To test this further, we varied in the gliding experiments the ionic strength while keeping the motor concentration constant. We observed a transition from plus- to minus-end–directed microtubule transport via an intermediate unstable regime upon increasing the ionic strength (figs. S6 and S7). This switch in directionality was again microtubule-length–dependent: Shorter microtubules underwent the transition from plus- to minus-end–directed motility at lower salt concentrations (fig. S6D) than did longer microtubules. This demonstrates that

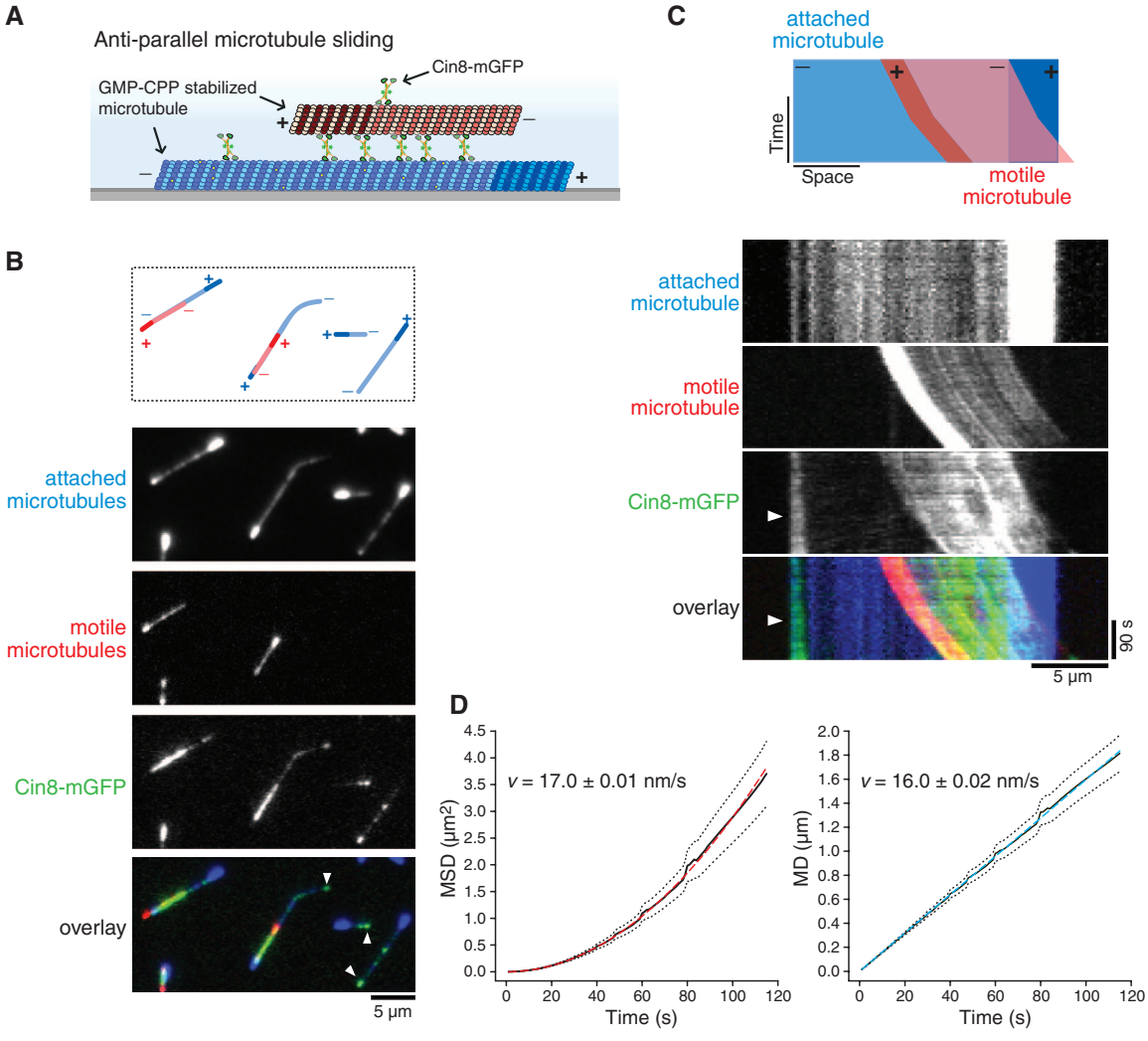

Fig. 2. Cin8 slides antiparallel microtubules apart in a plus-end–directed manner. (**A**) Scheme of the antiparallel sliding assay. (**B**) TIRF microscopy images showing (red) polarity-marked Alexa568-microtubules cross-linked to (blue) surface-immobilized polarity marked Alexa647-microtubules by (green) 4.5 nM of Cin8-mGFP in an antiparallel orientation. White arrowheads indicate Cin8-mGFP accumulation at the minus ends of surface-immobilized microtubules. (**C**) Example kymographs of a sliding antiparallel microtubule pair. (**D**) Quantification of antiparallel microtubule sliding. MSD and MD curves were calculated from tracks of sliding microtubules (n = 38 microtubules; n = 96 respective instantaneous velocities). Mean velocities (v) were derived by fitting the functions (dashed blue line) $MD = vt$ and (dashed red line) $MSD = v^2t^2$ to the data. Stated errors represent SEM. Dotted black lines in (D) are 95% confidence intervals.

the crucial parameter determining directionality of transport is not the ionic strength itself but rather is the number of mechanically coupled motors on the glass surface that interact with a microtubule. Increased salt concentrations weaken the motor-microtubule interaction and hence lower the number of microtubule-bound motors at a given surface density (*19*), supporting this interpretation. Directional switching did not require the entire tetrameric Cin8 protein, as demonstrated by using a C-terminally truncated Cin8 construct previously shown to be dimeric (fig. S8 and table S1) (*5*).

Minus-end–directed movement of Cin8 has not been observed in vivo. Because individual spindle microtubules cannot be visualized easily inside the yeast nucleus, we targeted GFP-labeled Cin8 to the cytoplasm by deleting the C-terminal nuclear localization signal (NLS) (*10*, *20*). This enabled us to observe Cin8 along single cytoplasmic microtubules. In all cells, Cin8 accumulated near the minus ends of cytoplasmic microtubules that are organized by the spindle pole body (SPB) (Spc72-mCherry) (Fig. 4, A and B, and fig. S9). Microtubule plus-end binding of Cin8 as reported previously (*10*) was rarely observed (<1%). The localization of cytoplasmic Cin8 was strongly microtubule-dependent (Fig. 4, A and B), making the possibility of a direct interaction of Cin8 with SPB components unlikely. Time-lapse imaging revealed short-lived microtubule binding events of Cin8 (Fig. 4C), which is in agreement with its in vitro dwell time and in contrast to the very processive plus-end–directed motility of Kip3 in vivo (Fig. 4D) (*21*, *22*). Thus, it is likely that Cin8 acts as a minus-end–directed motor on individual microtubules in vivo.

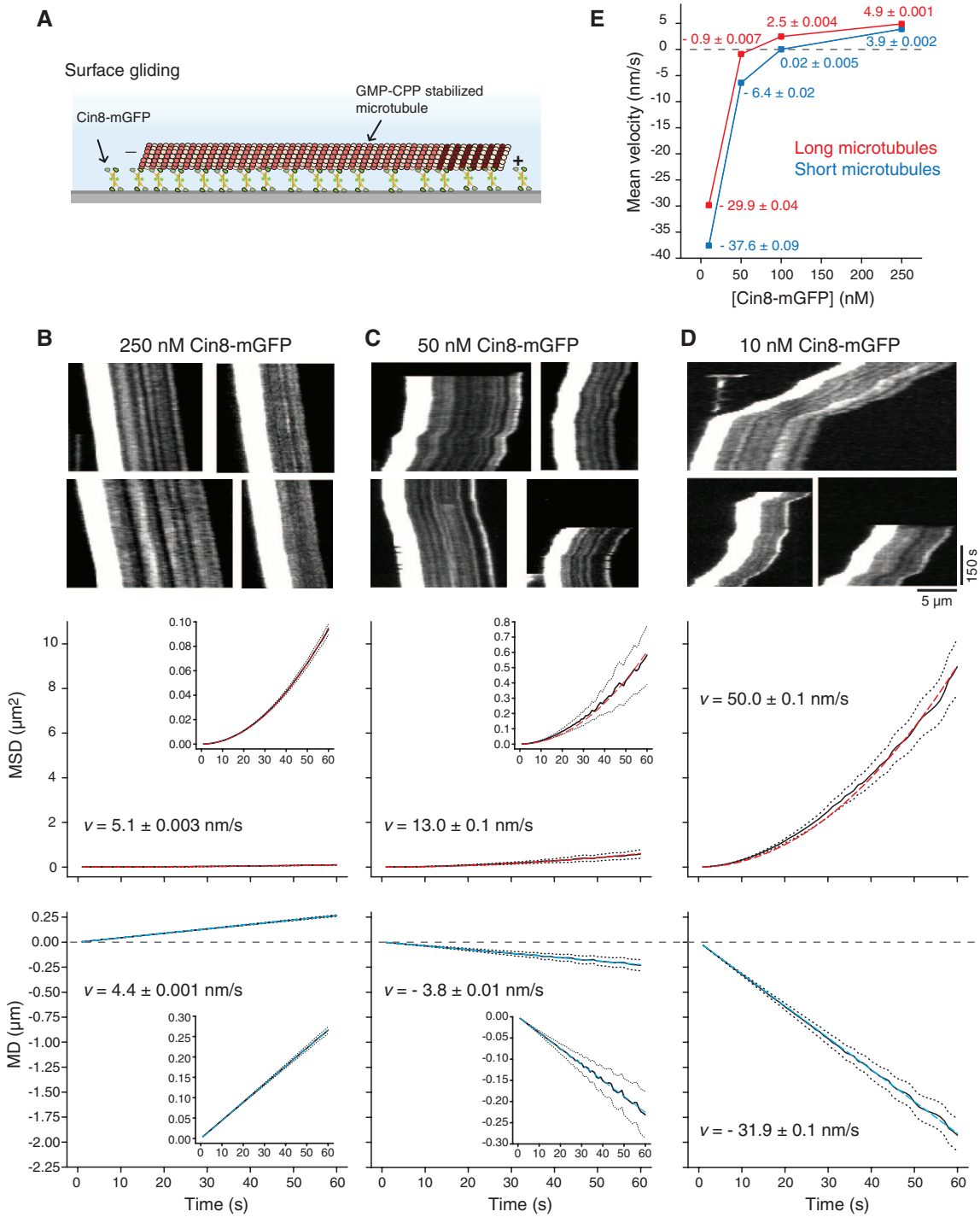

Fig. 3. Cin8 changes directionality depending on the number of microtubule-interacting motors. (**A**) Scheme of a surface gliding assay. (**B** to **D**) Example kymographs and quantifications of surface gliding assays performed at (B) 250, (C) 50, and (D) 10 nM Cin8-mGFP. MSD and MD curves were calculated from tracks of gliding microtubules. (**E**) Comparison of mean velocities between short (<8 µm) and long (>8 µm) microtubules at different motor concentrations (10, 50, 100, and 250 nM). Mean velocities were derived from MD fits, as described in Fig. 2D. Stated errors and error bars represent SEM. Dotted black lines on (B) to (D) are 95% confidence intervals.

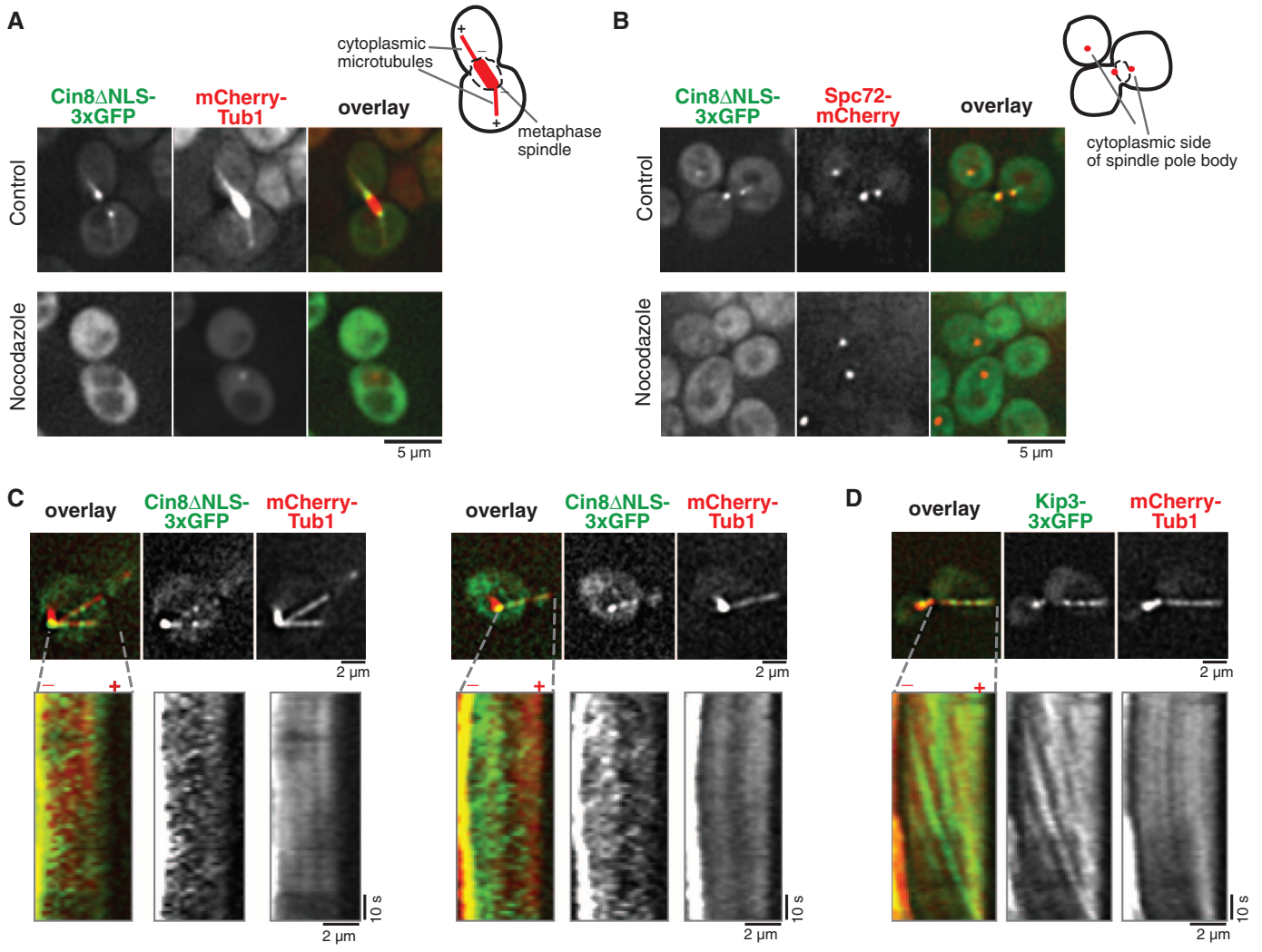

Fig. 4. Cin8 accumulates toward microtubule minus ends in vivo. Localization of cytoplasmic Cin8 (Cin8ΔNLS-3GFP) in cells with (**A**) labeled cytoplasmic microtubules (mCherry-Tub1) or (**B**) labeled cytoplasmic SPB component Spc72 (Spc72-mCherry; red) that anchors cytoplasmic microtubule minus ends. Dimethyl sulfoxide–treated control cells were compared with cells treated with the microtubule-depolymerizing drug nocodazole. Time-lapse analysis of (**C**) Cin8ΔNLS-3GFP and (**D**) Kip3-3GFP on cytoplasmic microtubules (mCherry-Tub1).

Similar to Cin8, kinesin-5 motors from fission yeast (*23*), *Xenopus* (*24*), and *Drosophila* (*25*) concentrate near spindle poles. Accumulation of plus-end–directed *Xenopus* kinesin-5 at the poles depends on the minus-end–directed motor dynein (*26*), which does not have a nuclear function in yeast. The minus-end–directed motility of Cin8 might bypass one of the functions that dynein has in higher eukaryotes.

Microtubule cross-linking promotes directional over diffusive motility of plus-end–directed *Xenopus* kinesin-5 (*27*). Here, Cin8 motors switched directionality in response to team size, suggesting that the ability to sense and respond to mechanical constraints might be a property of kinesin-5 motors, possibly because of specific features of this kinesin family (*28*, *29*). However, Cin8 is also an unusual member of the kinesin-5 family in containing a multitude of insertions and mutations in usually conserved regions (*29*, *30*).

In conclusion, Cin8 can switch between two distinct states of directional motility. On individual microtubules, single Cin8 motors preferentially move toward the minus end, whereas they switch to plus-end–directed movement when part of a large team of mechanically coupled motors cross-linking antiparallel microtubules. Such a context-dependent change in directionality is different from previously studied cases of bidirectionality (*14*, *31*).

References and Notes

1. N. Hirokawa, Y. Noda, Y. Tanaka, S. Niwa, *Nat. Rev. Mol. Cell Biol.* **10**, 682 (2009).
2. S. A. Endow, K. W. Waligora, *Science* **281**, 1200 (1998).
3. U. Henningsen, M. Schliwa, *Nature* **389**, 93 (1997).
4. H. Miki, Y. Okada, N. Hirokawa, *Trends Cell Biol.* **15**, 467 (2005).
5. E. R. Hildebrandt, L. Gheber, T. Kingsbury, M. A. Hoyt, *J. Biol. Chem.* **281**, 26004 (2006).
6. A. S. Kashina *et al.*, *Nature* **379**, 270 (1996).
7. L. C. Kapitein *et al.*, *Nature* **435**, 114 (2005).
8. M. A. Hoyt, L. He, K. K. Loo, W. S. Saunders, *J. Cell Biol.* **118**, 109 (1992).
9. D. M. Roof, P. B. Meluh, M. D. Rose, *J. Cell Biol.* **118**, 95 (1992).
10. M. K. Gardner *et al.*, *Cell* **135**, 894 (2008).
11. J. D. Tytell, P. K. Sorger, *J. Cell Biol.* **172**, 861 (2006).
12. A. Khmelinskii, J. Roostalu, H. Roque, C. Antony, E. Schiebel, *Dev. Cell* **17**, 244 (2009).
13. W. S. Saunders, D. Koshland, D. Eshel, I. R. Gibbons, M. A. Hoyt, *J. Cell Biol.* **128**, 617 (1995).
14. Materials and methods are available as supporting material on *Science* Online.
15. B. H. Kwok *et al.*, *Nat. Chem. Biol.* **2**, 480 (2006).
16. A. F. Straight, J. W. Sedat, A. W. Murray, *J. Cell Biol.* **143**, 687 (1998).
17. C. Hentrich, T. Surrey, *J. Cell Biol.* **189**, 465 (2010).
18. L. Gheber, S. C. Kuo, M. A. Hoyt, *J. Biol. Chem.* **274**, 9564 (1999).
19. P. Bieling, I. A. Telley, J. Piehler, T. Surrey, *EMBO Rep.* **9**, 1121 (2008).
20. E. R. Hildebrandt, M. A. Hoyt, *Mol. Biol. Cell* **12**, 3402 (2001).
21. M. L. Gupta Jr., P. Carvalho, D. M. Roof, D. Pellman, *Nat. Cell Biol.* **8**, 913 (2006).
22. V. Varga, C. Leduc, V. Bormuth, S. Diez, J. Howard, *Cell* **138**, 1174 (2009).
23. I. Hagan, M. Yanagida, *Nature* **356**, 74 (1992).
24. K. E. Sawin, K. LeGuellec, M. Philippe, T. J. Mitchison, *Nature* **359**, 540 (1992).
25. D. K. Cheerambathur, I. Brust-Mascher, G. Civelekoglu-Scholey, J. M. Scholey, *J. Cell Biol.* **182**, 429 (2008).
26. T. M. Kapoor, T. J. Mitchison, *J. Cell Biol.* **154**, 1125 (2001).
27. L. C. Kapitein *et al.*, *J. Cell Biol.* **182**, 421 (2008).

28. A. G. Larson, N. Naber, R. Cooke, E. Pate, S. E. Rice, *Biophys. J.* **98**, 2619 (2010).
29. J. Turner *et al*., *J. Biol. Chem.* **276**, 25496 (2001).
30. A. J. Bodey, M. Kikkawa, C. A. Moores, *J. Mol. Biol.* **388**, 218 (2009).
31. T. Guérin, J. Prost, P. Martin, J. F. Joanny, *Curr. Opin. Cell Biol.* **22**, 14 (2010).
32. We thank D. Pellman and M. Knop for plasmids; I. Hagan, J. Ellenberg, and M. Kaksonen for critically reading the manuscript; and the Deutsche Forschungsgemeinschaft, the European Commission (Marie Curie Research Training Network "Spindle Dynamics"), and the Swiss National Science Foundation for financial support.

Supporting Online Material
www.sciencemag.org/cgi/content/full/science.1199945/DC1
Materials and Methods
Supporting Text
Figs. S1 to S9
Tables S1 to S2
References
Movies S1 to S3

3 November 2010; accepted 11 February 2011
Published online 24 February 2011;
10.1126/science.1199945

The C-Terminal Domain of RNA Polymerase II Is Modified by Site-Specific Methylation

Robert J. Sims III,[1]*† Luis Alejandro Rojas,[1]* David Beck,[1] Roberto Bonasio,[1] Roland Schüller,[2] William J. Drury III,[1] Dirk Eick,[2] Danny Reinberg[1]‡

The carboxy-terminal domain (CTD) of RNA polymerase II (RNAPII) in mammals undergoes extensive posttranslational modification, which is essential for transcriptional initiation and elongation. Here, we show that the CTD of RNAPII is methylated at a single arginine (R1810) by the coactivator-associated arginine methyltransferase 1 (CARM1). Although methylation at R1810 is present on the hyperphosphorylated form of RNAPII in vivo, Ser2 or Ser5 phosphorylation inhibits CARM1 activity toward this site in vitro, suggesting that methylation occurs before transcription initiation. Mutation of R1810 results in the misexpression of a variety of small nuclear RNAs and small nucleolar RNAs, an effect that is also observed in *Carm1*$^{-/-}$ mouse embryo fibroblasts. These results demonstrate that CTD methylation facilitates the expression of select RNAs, perhaps serving to discriminate the RNAPII-associated machinery recruited to distinct gene types.

The carboxy-terminal domain (CTD) of the major subunit of RNA polymerase II (RNAPII) in mammals comprises 52 repeats of the consensus sequence Tyr-Ser-Pro-Thr-Ser-Pro-Ser (*1*). Although site-specific CTD phosphorylation mediates recruitment of other proteins to RNAPII, how this recruitment facilitates distinct processing events remains poorly understood (*2*–*4*). Nonconsensus repeats of the RNAPII CTD contain two arginine and seven lysine substitutions that primarily occur at position seven of the heptad motif. We hypothesized that such arginine and/or lysine residues might be targets for modification of the CTD of RNAPII and, as a consequence, engage activities associated with RNA production.

A glutathione *S*-transferase (GST)–CTD fusion protein containing repeats number 24–52 was not acetylated by HeLa-S3 nuclear extract as a source of enzymes, but specific methylation of the GST-CTD was observed, and its level correlated with increasing amounts of the extract (Fig. 1A). We purified the CTD methyltransferase enzyme from this extract (Fig. 1, B and C), detecting a band at ~65 kD that was crosslinked to a S-adenosyl methionine (SAM) after ultraviolet exposure (fig. S1B) (*5*). Mass spectrometric analysis revealed the presence of coactivator-associated arginine methyltransferase 1 (CARM1), which migrates at a molecular mass of approximately 65 kD by means of SDS–polyacrylamide gel electrophoresis (SDS-PAGE). To ascertain whether CARM1 was the enzyme that methylates the CTD, we performed methylation reactions using increasing amounts of recombinant CARM1 in the presence of the CTD and confirmed that CARM1 is capable of catalyzing this modification (Fig. 1D). Western blot analysis of the Superose 6 gel filtration fractions derived from conventional purification revealed that CARM1 and the CTD methyltransferase activity co-eluted (fig. S1C) (*5*). Given that we did not detect any CTD methyltransferase activity that fractionated apart from CARM1 during the purification and that nuclear extracts derived from *Carm1*$^{-/-}$ mouse embryonic fibroblasts (MEFs) were devoid of this activity (Fig. 1E), we concluded that CARM1 is the enzyme responsible for methylating the CTD. CARM1 is a type I protein arginine methyltransferase (PRMT) that catalyzes a methyltransferase reaction, producing asymmetric dimethylated arginine. Its substrates include histone H3 and p300, and it has been implicated in co-activation of nuclear receptor–directed transcription as well as in mRNA splicing (*6*, *7*), although the underlying mechanisms are largely obscure.

The largest subunit of RNAPII contains two arginine residues within the CTD; one is present within the N-terminal half of the CTD (R1603, second repeat), and the other within the C-terminal half (R1810, repeat number 31) (*8*). We tested whether both arginines are targets of CARM1 using methylation assays with GST fusion proteins containing either the N-terminal (GST-N-CTD) or C-terminal (GST-C-CTD) portions of the CTD. Only the GST-C-CTD substrate was methylated by recombinant CARM1, indicating that CARM1 targets R1810 (Fig. 2A). An alignment of the residues surrounding R1810 from different species suggests that CARM1 methylation may be conserved throughout evolution (Fig. 2B).

CARM1 methylated highly purified RNAP II derived from HeLa-S3 cells (Fig. 2C): Only the hypophosphorylated (IIA) form of RNAPII was methylated; the hyperphosphorylated form of RNAPII (IIO) was not. Methylation experiments by use of the CTD fusion protein that was prephosphorylated by Ser5- (CAK) or Ser2-specific (P-TEFb) kinases suggest that CARM1 methylation is sensitive to Ser2 and Ser5 phosphorylation (Fig. 2D). Furthermore, CARM1 was ineffectual when provided with synthetic peptides that were phosphorylated at Ser2 or Ser5 as substrates (Fig. 2, E and F). Phosphatase treatment of these peptides restored their ability to be methylated by CARM1 (Fig. 2G). The CTD of RNAPII is phosphorylated during the initiation of transcription; CARM1-mediated methylation probably takes place before phosphorylation, which is consistent with its recruitment during the early phases of transcriptional activation (*9*, *10*).

Immunofluorescence analyses performed on MEF cells by using a polyclonal antibody against a CTD peptide containing R1810me2a (fig. S2, A and B) showed that this modification is localized in the nuclei, which is similar to the case of phosphorylated CTD (anti-pSer5, clone 4H8) (Fig. 3A). *Carm1*$^{-/-}$ MEFs were devoid of CARM1, as expected (Fig. 3B) and also devoid of methylated CTD, as evidenced by the absence of signal using antibodies to CTDRme2a (anti-CTDRme2a) (Fig. 3A), which supports the conclusion that the CTD is methylated in vivo by CARM1. The anti-CTDme2a signal observed by using MEF cells was blocked by CTDme2a peptide but not by other synthetic peptides that are analog to CARM1 products, namely H3R26me2a or a symmetrically methylated peptide H4R3me2s (Fig. 3C). Using this antibody on Western blots, we detected methylation on hyperphosphorylated RNAPII purified from HeLa cells (Fig. 3D). Thus, CARM1

[1]Howard Hughes Medical Institute (HHMI), Department of Biochemistry, New York University School of Medicine, 522 First Avenue, Smilow 211, New York, NY 10016, USA. [2]Department of Molecular Epigenetics, Helmholtz Center Munich, Center of Integrated Protein Science Munich (CIPSM), Marchioninistrasse 25, 81377 Munich, Germany.

*These authors contributed equally to this work.
†Present address: Constellation Pharmaceuticals, Cambridge, MA 02139, USA.
‡To whom correspondence should be addressed. E-mail: danny.reinberg@nyumc.org

Directional Switching of the Kinesin Cin8 Through Motor Coupling

Johanna Roostalu, Christian Hentrich, Peter Bieling, Ivo A. Telley, Elmar Schiebel and Thomas Surrey

Science **332** (6025), 94-99.
DOI: 10.1126/science.1199945originally published online February 24, 2011